I&EC research
Industrial & Engineering Chemistry Research
pubs.acs.org/IECR
Article

Thiol- and Amine-Incorporated UIO-66-NH_2 as an Efficient Adsorbent for the Removal of Mercury(II) and Phosphate Ions from Aqueous Solutions

Fathi S. Awad, Ayyob M. Bakry,* Amr Awad Ibrahim, Andrew Lin, and M. Samy El-Shall*

Cite This: *Ind. Eng. Chem. Res.* 2021, 60, 12675−12688

ABSTRACT: In this study, the novel adsorbent UIO-66-IT was synthesized to extract mercury and phosphate ions from contaminated water. The synthetic strategy involved the preparation of the metal−organic framework (UIO-66-NH_2) followed by post-synthetic modification using the chelating ligand 2-imino-4-thiobiuret to form the UIO-66-IT adsorbent. The structure and the morphology of the adsorbent were investigated by a variety of analytical techniques including Fourier transform infrared, X-ray diffraction, X-ray photoelectron spectroscopy, scanning electron microscopy, transmission electron microscopy, and Brunauer−Emmett−Teller surface area measurements. The adsorption of mercury and phosphate was optimized by studying the effect of pH, initial concentration, contact time, dose, temperature, and competitive ions. The results revealed exceptionally high adsorption capacities toward mercury and phosphate ions of 580 and 178 mg/g, respectively, at pH = 5.5 and an initial concentration of 1500 and 1000 mg/L. The adsorption isotherms are in excellent agreement with the Langmuir isotherm model, indicating the formation of a monolayer on the surface of UIO-66-IT. The kinetics of adsorption fit well with the pseudo-second-order kinetics model, which suggests the chemical adsorption of mercury ions via the nitrogen and sulfur functional groups of the adsorbent and the physical adsorption of phosphate anions by protonated functional groups on the surface of the UIO-66-IT adsorbent. Selectivity studies showed removal efficiencies of 98.9% Hg(II) from a solution containing a mixture of metal ions at 25 mg/L. Regeneration studies showed that the adsorbent can be recycled several times by using nitric acid for mercury removal and sodium chloride for phosphate removal. Removal efficiencies were higher than 99% for both regenerations. Due to the simple synthetic strategy via cost-effective starting materials, unique chemical structure, rapid adsorption kinetics, and high surface area, which lead to excellent removal efficiency, stability, and excellent regeneration, UIO-66-IT is introduced as a unique adsorbent for the selective removal of mercury and phosphate ions to remediate polluted water.

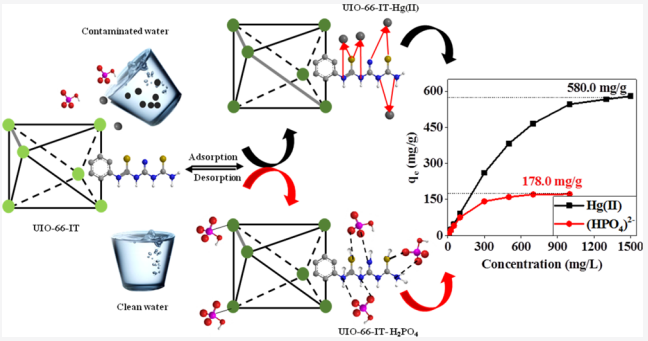

1. INTRODUCTION

Mercury is recognized as a top toxic heavy metal found in different forms including organic and inorganic compounds. This toxic element can contaminate drinking water sources through industrial and chemical waste, which arises as a consequence of the development of new technology. According to the United States Environmental Protection Agency (EPA) regulations, mercury concentration in drinking water sources is limited to less than 2 μg/L due to various fatal health issues such as organ dysfunction and chronic diseases, which can occur when mercury concentrations exceed this limit.[1,2] Similarly, phosphates are one of the most used intermediates in the chemical industry to produce different products including detergents, food products, and fertilizers. As a result of using phosphate-containing chemicals, a large quantity of phosphate products is released to drinking water sources and can cause the rapid growth of algae and aquatic plants in drinking water resources.[3] Therefore, the removal of both phosphate and mercury from industrial waste before the contamination of drinking water sources has become a hot topic for scientific research in recent years.

Different approaches have been used to purify water from phosphate and mercury including chemical, physical, and biological methods. The most efficient and cost-effective approaches are chemical methods such as ion exchange, membrane filtration, chemical precipitation, and adsorption. The adsorption method has attractive advantages (such as ease in operation and applications, low cost, and scalability) when compared to other methods that are expensive or not efficient

Received: May 21, 2021
Revised: August 10, 2021
Accepted: August 12, 2021
Published: August 24, 2021

https://doi.org/10.1021/acs.iecr.1c01892
Ind. Eng. Chem. Res. 2021, 60, 12675−12688

in some cases.[1,4] Therefore, many reported adsorbents have been used to clean contaminated water sources. Most of the adsorbents achieved high adsorption capacities in short periods and high selectivity to specific metal ions in the solution. These adsorbents include graphene oxide,[5] activated carbon,[6] carbon nanotubes,[7] nitrogen-doped carbon,[8] silica,[9] chemically modified bioadsorbents,[10,11] polymers,[12] covalent organic frameworks,[13,14] and metal organic frameworks (MOFs).[15]

MOFs are a class of porous nanomaterials composed of inorganic clusters linked by organic linkers to form a porous network. They exhibit tunable properties such as high surface area, tunable porosity, and the ability to be synthesized and functionalized in different ways. These properties make MOFs exceptional materials to be used in different applications including drug delivery, gas storage, heterogeneous catalysis, sensors, and adsorption. In recent years, MOFs have been used as adsorbents in water treatments and the results revealed that some MOFs are stable in water and show promising adsorption capacities for the removal of heavy metals and different poisoning ions from water.[16] The most commonly reported MOFs in the literature for this purpose are MIL-53(Al), AMOF-1, ZIF-8, ZIF-67, Chitosan MOF, MOF-808, TMU-5, TMU-30, TMU-101, Cu-terephthalate-MOF, UIO-67, UIO-66, and UIO-66-NH_2. All these MOFs were reported in the literature for water purification from heavy metals.[17,18]

The applications of zirconium-based MOFs (UiO-66-X, where X can be SO_3H, NH_2, COOH, H, etc.) have attracted great attention due to their exceptional water stability and high adsorption capacities.[19−22] UiO-66-NH_2 exhibits no significant changes in the X-ray diffraction (XRD) pattern and the crystalline structure after exposure to liquid water and other solvents due to inorganic unit strength, where each $Zr_6O_4(OH)_4$ unit is 12-coordinated to terephthalic acid ligands.[20−22] Therefore, in this study, UiO-66-NH_2 was selected as an adsorbent for the removal of heavy metals from wastewater because of its high stability in water and over a wide pH range (1−14).[20−22] Additionally, NH_2 groups in UiO-666-NH_2 have free lone pairs of electrons and can act as a Lewis base and form coordinate bonds with metal ions (Lewis acids).[22] Recently, there have been efforts to chemically functionalize UiO-66-NH_2 with strong chelating ligands to increase the adsorbent selectivity and capacity toward heavy metals.[16,23,24] For examples, UIO-66-thiol,[25] UIO-66-$(SH)_2$,[26] UIO-66-2,5-dimercapto-1,3,4-thiadiazol,[27] UIO-66-Cys,[28] UIO-66-NHC(S)NHME,[29] and UIO-66-Syst[30] were utilized to purify polluted water from mercury and the results showed the maximum removal efficiencies of 171.5, 263.4, 670.5, 350.1, 769.0, and 110.5 mg/g, respectively. Moreover, Zr-MOFs have been utilized to purify water from phosphate ions due to the high affinity of Zr to interact with phosphate ions. For illustrations, UIO-66,[31] UIO-66-NH_2,[31] UIO-66-3PEI,[32] UIO-NO_2,[33] and UIO-66-Br[33] were applied to remediate contaminated water from phosphate ions and the results showed the maximum removal efficiencies of 85.0, 92.5, 73.1, 117.7, and 132.5 mg/g, respectively. Therefore, UIO-66 and its modified derivatives have plenty of applications in water purification from mercury and phosphate ions from aqueous solutions.

In this work, the novel adsorbent UIO-66-IT was synthesized from UIO-66-NH_2 by post-synthetic modification to incorporate 2-imino-4-thiobiuret (IT) as a chelating ligand for the removal of mercury and phosphate ions from wastewater. The chelating ligand IT was chosen due to its abundant nitrogen and sulfur functional groups, cost efficiency compared to other ligands, and its practical applications in the removal of heavy metals from wastewater.[2,34] The synthetic strategy has been accomplished in two main steps. First, UIO-66-NH_2 was converted to UIO-66-NCS through the primary amine functional groups using thiophosgene as a coupling agent. Then, a nucleophilic addition reaction took place between the isothiocyanate group of UIO-66-NCS and the primary amine groups on the IT chelating ligand to yield UIO-66-IT.[29,35,36] Fourier transform infrared (FTIR), XRD, X-ray photoelectron spectroscopy (XPS), scanning electron microscopy (SEM), transmission electron microscopy (TEM), and Brunauer−Emmett−Teller (BET) surface area measurements were employed to prove the chemical attachment of the IT chelating ligand on UIO-66-NH_2 and the morphology of the prepared adsorbent. This adsorbent was utilized to adsorb Hg(II) and $(HPO_4)^{2-}$ ions from contaminated water. The adsorption conditions were optimized by varying the following factors: pH, initial concentration of phosphate and mercury ions, adsorbent dosage, reaction contact time, and types of interfering ions. The experimental results were explained by the Langmuir adsorption isotherm and the pseudo-second-order kinetic modules, while the adsorption mechanisms were investigated by using XPS analyses. The UIO-66-IT adsorbent was specifically chosen for the removal of Hg(II) and $(HPO_4)^{2-}$ ions due to its simple synthetic strategy via cost-effective starting materials and a unique chemical structure that contains a IT chelating ligand, with nitrogen and sulfur heavy donor atoms acting as active adsorption sites within a high surface area of 735 m^2/g of the porous MOF structure. Moreover, the adsorbent showed high removal efficiency with fast adsorption kinetics, excellent regeneration, and reusability. Therefore, UIO-66-IT is introduced as a unique adsorbent for the selective removal of mercury and phosphate ions to remediate polluted water.

2. EXPERIMENTAL SECTION

2.1. Materials. All chemicals were acquired commercially from Sigma-Aldrich, and they were of analytical grade, therefore, they were used without further purification. These chemicals include 2-aminoterephthalic acid (99%), zirconyl chloride (99.5%), tetrahydrofuran (THF) (99%), thiophosgene (99.5%), anhydrous dimethylformamide (99.9%), acetonitrile (99%), IT (96%), sodium hydroxide (99%), nitric acid (99%), and hydrochloric acid (99%). $HgCl_2$, $Pb(NO_3)_2$, $CuCl_2{\cdot}2H_2O$, $Ni(NO_3)_2{\cdot}6H_2O$, $FeCl_2$, and $AlCl_3$ were used as sources of Hg(II), Pb(II), Cu(II), Ni(II), Fe(II), and Al(III) cations, respectively. Na_2HPO_4, NaCl, and $NaNO_3$ were used as sources of $(HPO_4)^{2-}$, Cl^-, and $(NO_3)^-$ anions, respectively. Deionized water (DI water) was used to prepare all studied stock solutions.

2.2. Synthesis of UIO-66-IT. UIO-66-NH_2 was synthesized from 2-aminoterephthalic acid and zirconyl chloride using previously reported conditions.[24] To prepare UIO-66-NCS, 100 mg of UIO-66-NH_2 was suspended in 50 mL of THF in a 100 mL round bottom flask followed by the addition of 1 mL of thiophosgene. Then, the flask was connected to a condenser with a magnetic stirrer at 55 °C for 18 h. The product was washed five times with THF and dried for 24 h at 100 °C. To prepare UIO-66-IT, a mixture of 100 mg of UIO-66-NCS and 300 mg of IT was placed in a 100 mL round bottom flask. Then, 50 mL of acetonitrile was added to the flask and the mixture was sonicated for 1 h. After that, the flask

https://doi.org/10.1021/acs.iecr.1c01892
Ind. Eng. Chem. Res. 2021, 60, 12675−12688

Scheme 1. General Synthetic Strategy to Prepare UIO-66-IT

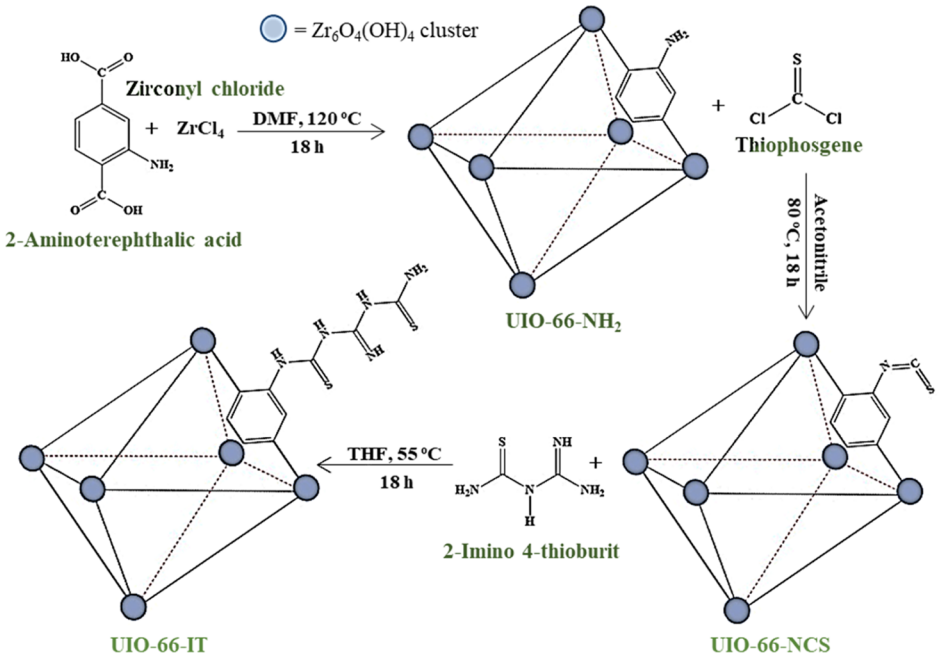

was connected to a condenser with a magnetic stirrer at 55 °C for 18 h. The product was washed three times with acetonitrile and dried for 24 h at 100 °C.[37,38]

2.3. Instrumentation. UIO-66-NH_2, UIO-66-NCS, and UIO-66-IT were characterized by the powder XRD patterns of the adsorbents, which were measured at room temperature using the PANalytical MPD X'Pert PRO diffractometer with the voltage of 45 kV and current 40 mA via a Ni-filtered Cu Kα_1 radiation. The XPS spectra of the materials were obtained using a Thermo Fisher Scientific ESCALAB 250 spectrometer with a microfocused monochromated Al Kα X-ray source (15 kV) and a double-focusing full 180° spherical sector electron analyzer. FTIR spectroscopy was carried out using the Nicolet-Nexus 670 FTIR spectrometer (4 cm^{-1} resolution and 32 scans) diamond attenuated total reflectance. SEM images were taken using the Hitachi SU-70 field-emission SEM with an energy of 5.0 kV. TEM images were obtained at 100 kV by a JEOL JEM-1400 transmission electron microscope. The concentrations of heavy metals in the solutions before and after removal experiments were quantified by either the Varian Vista-MPX inductively coupled plasma optical emission spectroscopy (ICP−OES) with Ar^+ ion plasma gas equipped with a charged coupled detector for simultaneous detection at parts per million (ppm) concentration levels or with the Agilent 8900 triple quadrupole ICP−MS with Ar^+ ion plasma gas and an electron multiple detector for the detection of toxic metals at parts per billion (ppb) levels.

2.4. Adsorption and Desorption Experiments. Adsorption and desorption of heavy metals from contaminated water were determined in the experiments by using 5 mL of toxic metal solution and 5 mg of the adsorbent in 20 mL glass vials at various pH, initial concentrations, and contact time. The samples were acidified with 2% HNO_3 before analysis, and either ICP−OES or ICP−MS was used to measure the concentration of heavy metal ions in the solutions after removal or desorption experiments at ppm or ppb levels, respectively. The adsorption capacity, removal efficiency, desorption capacity, and desorption efficiency were calculated from the following eqs 1−4, respectively.[2,13]

$$q_e = \frac{(C_0 - C_e)V}{m} \quad (1)$$

$$\%\, R_e = \frac{(C_0 - C_e)}{C_0} \times 100 \quad (2)$$

$$q_d = \frac{C_d V}{m} \quad (3)$$

$$\%\, D_e = \frac{q_d}{q_e} \times 100 \quad (4)$$

where q_e is the adsorption capacity (mg/g), C_0 is the initial concentration of heavy metal ions in the solution (mg/L), C_e is the equilibrium concentration (mg/L) after adsorption, V is the volume of the solution of metal ions (L) and m is the mass of the adsorbent (g), % R_e is the percentage of removal (%), q_d is the desorption capacity in (mg/g), C_d is the concentration of heavy metal ions in the eluent in (mg/L) after the adsorption experiment, and % D_e is the desorption efficiency (%).

2.5. Toxic Metal Removal Experiments. The effect of pH was investigated by changing the pH of the solutions within the range of 3−6 by using 0.1 M NaOH and 0.1 M HCl. The effect of concentration was determined by adjusting the concentration of the solutions between 10 and 1500 mg/L at the ppm level or 10−500 μg/L at the ppb level for Hg(II). Phosphate concentrations were adjusted between 10 and 1000 mg/L for the ppm level. The effect of contact time was studied by measuring uptake of the toxic metals as a function of time at initial concentrations of 100 mg/L. The effect of temperature for Hg(II) and $(HPO_4)^{2-}$ was carried out by varying the temperature between 20 and 50 °C. The effect of the amount of UIO-66-IT was studied at 1000 mg/L for Hg(II) ions and 500 mg/L for $(HPO_4)^{2-}$ ions. The selectivity of the adsorbents toward specific metal ions was investigated using a mixture containing six metal cations including Hg(II), Pb(II), Cu(II),

https://doi.org/10.1021/acs.iecr.1c01892
Ind. Eng. Chem. Res. 2021, 60, 12675−12688

Ni(II), Fe(II), and Al(III) at pH = 5.5 and concentrations of 300 and 10 mg/L. A mixture containing three anions- $(HPO_4)^{2-}$, Cl^-, and $(NO_3)^-$ was used to study the selectivity of the adsorbents toward specific anions at concentrations of 0.5 and 100 mg/L. The desorption of Hg(II) ions from the surface of UIO-66-IT was achieved by using different concentrations of HCl and thiourea, while $(HPO_4)^{2-}$ by using sodium chloride to regenerate the adsorbent.

3. RESULTS AND DISCUSSION

3.1. Materials Design. The design strategy to prepare UIO-66-IT is accomplished in three main steps, as they are summarized in Scheme 1. The first step is the preparation of UIO-66-NH_2 by using 2-aminoterephthalic *acid* and $ZrCl_4$ to produce UIO-66-NH_2 through solvothermal synthesis. In this step, the inorganic clusters [face-centered arrangement of cubic $Zr_6O_4(OH)_4$] coordinate with the 2-aminoterephthalic acid organic linkers through carboxylic acid functional groups, resulting in the adsorbent functionalized with free primary amines, UIO-66-NH_2.[39] The second step is a post-synthetic modification of UIO-66-NH_2 using thiophosgene to get UIO-66-NCS. This step involves a reaction between the nucleophilic primary amines on UIO-66-NH_2 and the electrophilic carbon atoms from thiophosgene to yield UIO-66-NCS by the elimination of HCl at 80 °C.[40] The final step is the attachment of the chelating ligand IT on the surface of UIO-66-NCS. This reaction involves nucleophilic attack of the electrophilic isothiocyanate groups on UIO-66-NCS, which results in electron shifts, proton loss, and creation of a thiourea linkage between the IT amine groups and isothiocyanate on UIO-66-NCS with no leaving group involved.[36]

3.2. Characterizations. The crystallinity of the prepared adsorbents was studied using XRD analysis, and the results are depicted in Figure 1 for UIO-66-NH_2, UIO-66-NCS, and UIO-66-IT. It is clearly seen that all materials are crystalline and have very similar XRD diffraction patterns at 2θ = 7.4, 8.6, and 25.8° due to (111), (200), and (600) diffraction planes, respectively. These results prove that the chemical modifications of UIO-66-NH_2 by both thiocyanate and IT chelating ligands did not affect the crystallinity of the UIO-66-NH_2 MOF.[29,41]

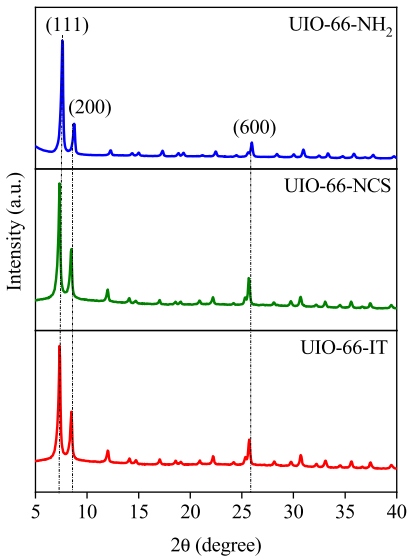

Figure 1. XRD patterns of UIO-66-NH_2, UIO-66-NCS, and UIO-66-IT.

The surface functional groups on UIO-66-NH_2, UIO-66-NCS, and UIO-66-IT were first analyzed by FTIR spectroscopy, and the results are shown in Figure 2A,B. The results showed that all materials have common peaks at 550, 670, and 760 cm^{-1} due to Zr−O_2 vibrations. Also, there are three characteristic peaks at 1770, 1570, and 1420 cm^{-1}, which belong to C═O, COO^-, and O−C−O bond vibrations, respectively. However, both UIO-66-NH_2 and UIO-66-IT have common peaks at 3000−3500, 1660, and 1253 cm^{-1} due to N−H stretching, N−H bending, and C−N bending, respectively. Similarly, UIO-66-NCS and UIO-66-IT have characteristic peaks, which are not present in UIO-66-NH_2 that prove the successful post functionalization of the UIO-66-NH_2 MOF. These peaks appeared at 2122, 1040, and 1073 cm^{-1} due to the stretching and bending modes of C═S and C−S bonds.[27,41,42]

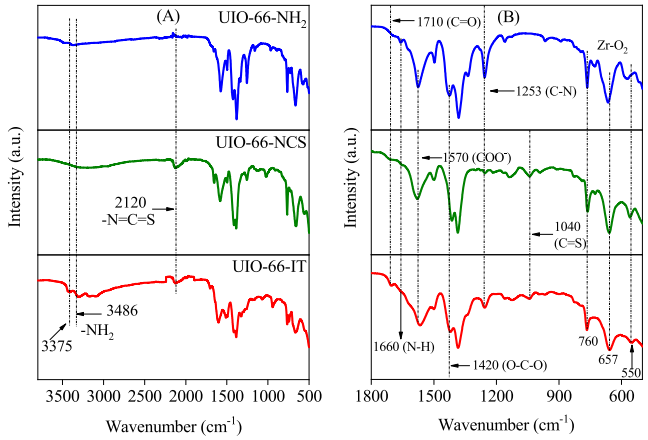

Figure 2. (A) FTIR spectra of UIO-66-NH_2, UIO-66-NCS, and UIO-66-IT and (B) specific region (600−1800 cm^{-1}).

XPS analysis was used to confirm FTIR results. The survey spectra of UIO-66-NH_2, UIO-66-NCS, and UIO-66-IT are plotted in Figures S1A, S2A, and 3A, respectively. The results showed that all materials have Zr, C, N, and O, but UIO-66-NCS and UIO-66-IT have S in addition to the previous elements, which confirm the post-synthetic modification of UIO-66-NH_2 by thiocyanate and IT chelating ligands.[2,27] The high-resolution C 1s spectra of UIO-66-NH_2, UIO-66-NCS, and UIO-66-IT are depicted in Figures S1B, S2B, and 3B, respectively. The results showed that both UIO-66-NH_2 have three characteristic peaks at binding energy values of 284.6, 285.5, and 288.6 eV, which were attributed to C−C/C═C, C−O/C−N, and O−C═O, respectively. Similarly, C 1s in UIO-66-NCS was deconvoluted into three peaks at 284.6, 285.7, and 288.6 eV due to C−C/C═C, C−O, and O−C═O/C═N/C═S, respectively. However, C 1s in UIO-66-IT has four characteristic peaks at binding energy values of 284.6, 285.2, 285.7, and 288.6 eV due to C−C/C═C, C−N, C−O/C−S, and O−C═O/C═N/C═S, respectively.[43] Furthermore, O 1s in UIO-66-NH_2, UIO-66-NCS, and UIO-66-IT is depicted in Figures S1C, S2C, and 3C respectively. The results showed that all materials have similar spectra at binding energy values of 530.8 and 532.8 eV due to Zr−O_2 and O−C═O, respectively. Similarly, Zr 3d shown in Figures S1D, S2D, and 3D for UIO-66-NH_2, UIO-66-NCS, and UIO-66-IT, respec-

https://doi.org/10.1021/acs.iecr.1c01892
Ind. Eng. Chem. Res. 2021, 60, 12675−12688

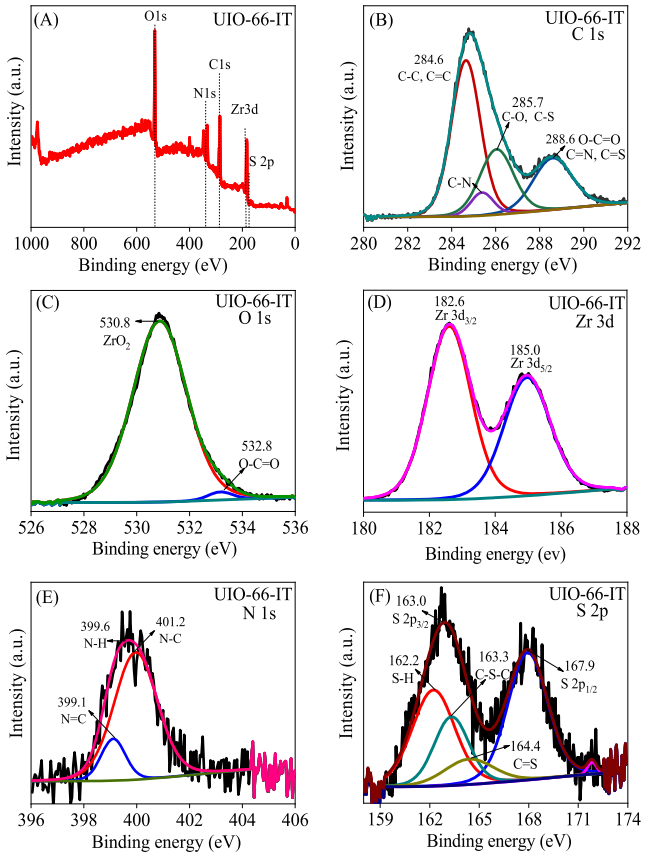

Figure 3. XPS spectra of UIO-66-IT (A) and survey spectrum of (B) C 1s, (C) O 1s, (D) Zr 3d, (E) N 1s, and (F) S 2p.

tively, was deconvoluted into Zr $3d_{3/2}$ and Zr $3d_{5/2}$ at binding energy values of 182.6 and 185.0, respectively.[27,29] From O 1s and Zr 3d XPS results, it is clearly seen that the post-synthetic modification did not take place on O and Zr functional groups.

The successful incorporation of the IT chelating ligand on UIO-66-NH_2 is also evident by the N 1s and S 2p spectra shown in Figures S1E, S2E, and 3E for UIO-66-NH_2, UIO-66-NCS, and UIO-66-IT, respectively. The N 1s spectrum in UIO-66-IT was deconvoluted into three peaks at binding energies of 399.1 eV (N in N═C bonds), 399.6 eV (N in C−N bonds), and 401.2 eV (N in C−N−C or C═N bonds), while UIO-66-NCS has only one peak at 399.1 due to (C═N bond), and UIO-66-NH_2 was deconvoluted into two peaks. Similarly, the S 2p spectrum is shown in Figures 3F and S2F for UIO-66-IT and UIO-66-NCS, respectively. The results showed that both materials have S $2p_{3/2}$ and S $2p_{1/2}$, but UIO-66-IT is fitted to three peaks at binding energies of 162.2 eV (S in S−H bonds), 163.3 eV (S in C−S−C bonds), and 164.4 eV (S in C═S bonds).[2,25,27] Therefore, the C 1s, N 1s, and S 2p XPS spectra of IT-PRGO provide clear evidence for the presence of C−S−C, and C−S, and C−N covalent bonds within the surface of the UIO-66-IT nanosheets.

The porosity and the surface area of UIO-66-NH_2, UIO-66-NCS, and UIO-66-IT were determined using nitrogen adsorption−desorption isotherms. The results of adsorption isotherms and pore volume are depicted in Figure 4A,B, while the calculated parameters are summarized in Table 1. The

Table 1. Surface Area and Pore Volume of UIO-66-NH_2, UIO-66-NCS, and UIO-66-IT

sample	surface area (m2/g)	pore volume (cm^3/g·Å)
UIO-66-NH2	1132	0.406
UIO-66-NCS	856	0.238
UIO-66-IT	735	0.221

results revealed that all samples have a typical type 1 adsorption isotherm and are microporous. The BET surface area of UIO-66-NH_2 was found to be 1132 m^2/g, while after post-synthetic modifications, this value reduced to be 856 m^2/g for UIO-66-NCS and 735 m^2/g for UIO-66-IT. The reduction in the surface area values is attributed to the degree of post-synthetic modification and the size of the substituent, in which both play huge roles in the adsorption of nitrogen molecules on the surface. Therefore, UIO-66-IT has a less surface area than UIO-66-NH_2, which can be attributed to the conversion of the amine groups to the bulkier imino-thiobiuret groups.[27,29]

SEM images shown in Figure 5A,B and TEM images shown in Figure 5C,D for UIO-66-IT show that the adsorbent has an octahedral morphology with a particle size of less than 200 nm. These images also resemble SEM and TEM images shown in Figures S3 and S4 for UIO-66-NH_2, and UIO-66-NCS, respectively. Therefore, the similarities in the crystallinity, as well as the morphology, indicate the stability of UIO-66-NH_2 under the post-synthetic modification to form isothiocyanate or IT-functionalized UIO-66-MOFs.[25,27]

The combination of the abovementioned characterization results, particularly FTIR, and XPS spectra provide strong evidence for the formation of UIO-66-IT from UIO-66-NH_2 through two main steps. The first step is to convert UIO-66-NH_2 amine groups into isothiocyanate, and the second step involves chemical reactions between $-NH_2$ or −SH groups from the IT chelating ligand and the isothiocyanate groups of

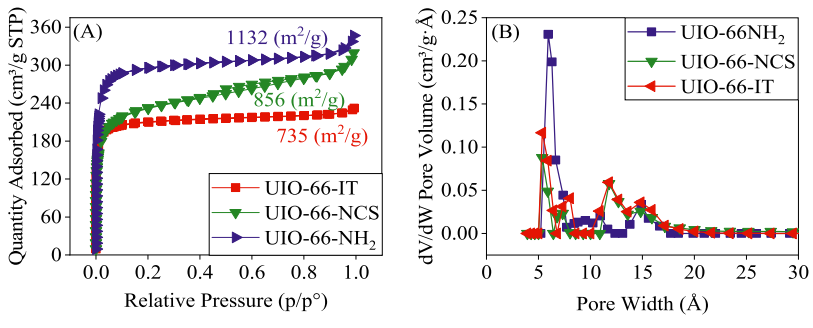

Figure 4. (A) Adsorption−desorption isotherms and (B) estimated pore size of UIO-66-NH_2, UIO-66-NCS, and UIO-66-IT.

https://doi.org/10.1021/acs.iecr.1c01892
Ind. Eng. Chem. Res. 2021, 60, 12675−12688

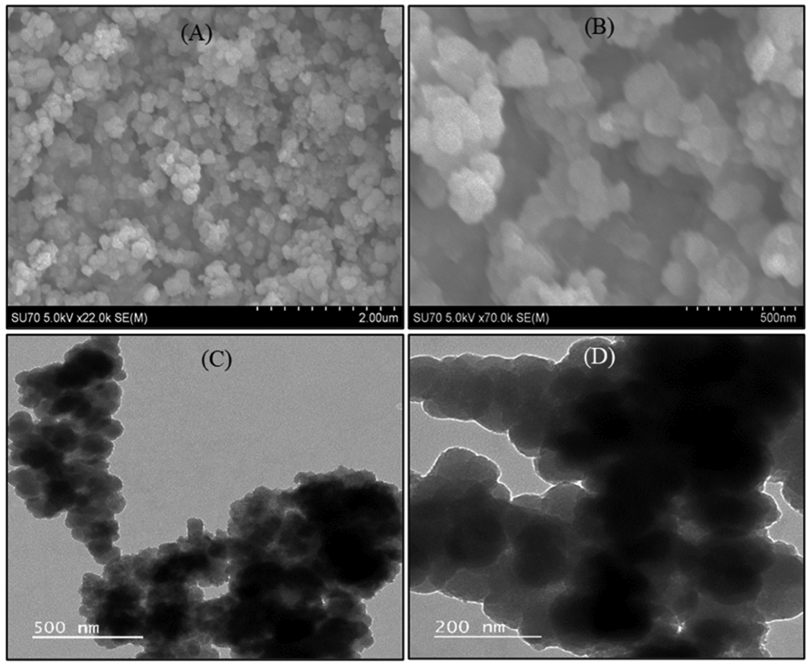

Figure 5. (A,B) SEM images and (C,D) TEM images of UIO-66-IT.

Scheme 2. Two Possible Pathways for the Reaction between Isothiocyanate and IT to Form UIO-66-IT

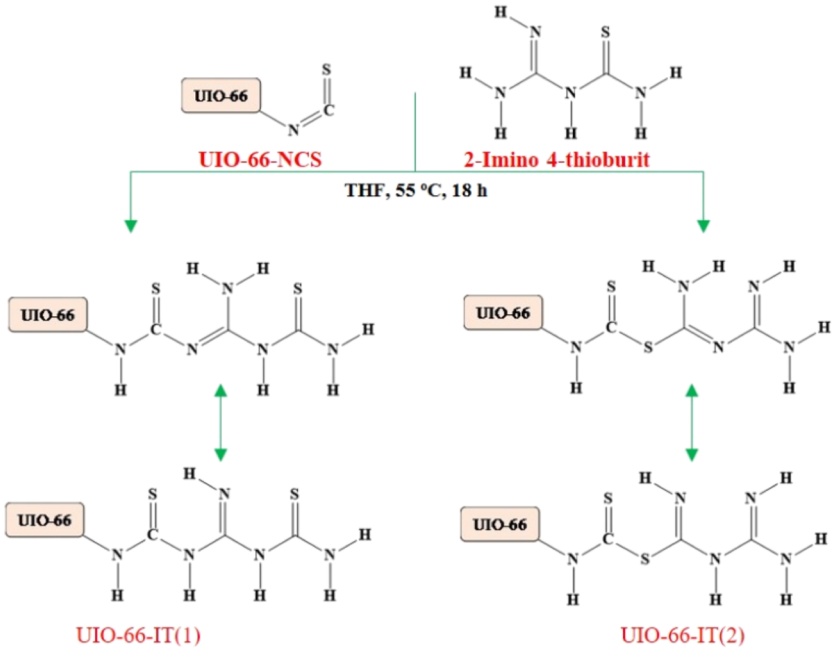

UIO-66-NCS. Therefore, two possible structures of UIO-66-IT can be suggested, as shown in Scheme 2.

3.3. Adsorption Studies. *3.3.1. Effect of pH.* The effect of pH on the removal of Hg(II) and $(HPO_4)^{2-}$ on UIO-66-IT was studied using a pH range of 3−6. The results plotted in Figure 6A indicate that as the pH of the solutions increases from 3 to 6, the adsorption capacity increased to the maximum values at pH 4−6 for $(HPO_4)^{2-}$ and pH 5−6 for Hg(II). The low adsorption capacities for Hg at low pH were attributed to the presence of hydrogen ions that would interfere with the adsorption process via competition with mercury ions for the sorbent surface binding sites. The low adsorption capacity for phosphate ions at low pH was attributed to the presence of phosphate ions as H_3PO_4, which naturally decreases the electrostatic interaction with adsorbent active sites.[27,31]

3.3.2. Effect of Concentration and Adsorption Isotherms. The effect of the initial concentration on the removal of Hg(II) and $(HPO_4)^{2-}$ ions was studied using the following constant conditions: T = 289 K, pH = 5.5, t = 6 h, and dose = 5 mg/L. The concentrations for Hg(II) were varied within two ranges (50−500 μg/L and 5−1500 mg/L). Phosphate ion concentrations were varied between 5 and 500 mg/L. The results plotted in Figure 6B for Hg(II) at the concentration range of 50−500 μg/L indicate a removal efficiency of 100%. This is attributed to the low concentrations of Hg(II) in the solution and the abundant active sites on the adsorbent.[27] To measure

https://doi.org/10.1021/acs.iecr.1c01892
Ind. Eng. Chem. Res. 2021, 60, 12675−12688

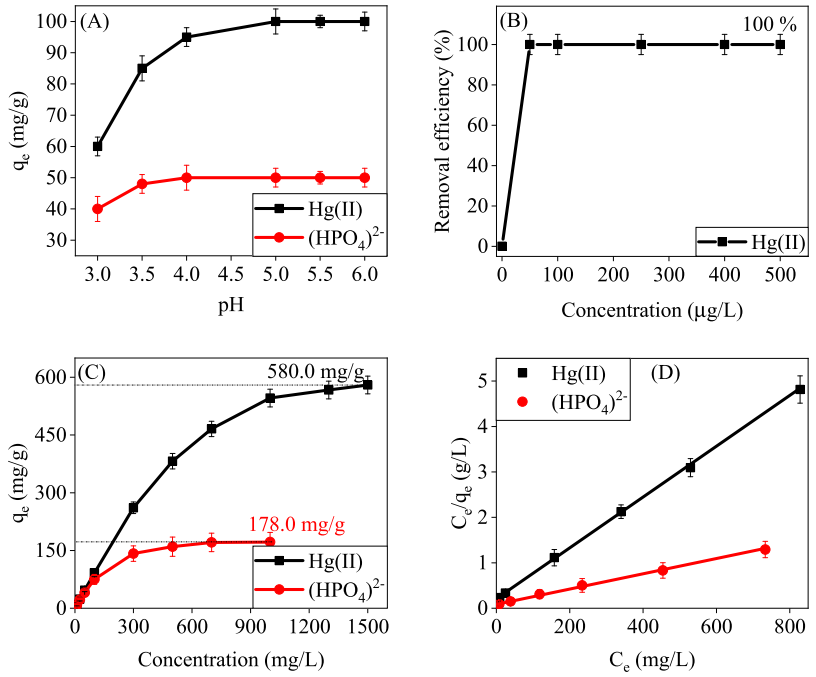

Figure 6. Removal of Hg(II) and $(HPO_4)^{2-}$ on UIO-66-IT. (A) Effect of pH [conditions; C_0 = 100 mg/L Hg(II), 50 mg/L $(HPO_4)^{2-}$, pH = 3.0−6.0], (B) effect of initial concentration on the removal of Hg(II) C_0 = 5−500 μg/L, (C) effect of initial concentration on the removal of Hg(II) C_0 = 10−1500 mg/L and $(HPO_4)^{2-}$ C_0 = 10−1000 mg/L, (conditions; pH = 5.5, T = 289 K, t = 6 h, and dose = 5 mg/5 mL), and (D) Langmuir adsorption isotherm module.

the maximum adsorption capacities (q_{max}), the concentrations were increased to ppm, as shown in Figure 6C. The adsorption capacities for both Hg(II) and $(HPO_4)^{2-}$ increased rapidly at the beginning of the adsorption process. As the concentration increased, the adsorption capacities reached saturation (q_{max}). The maximum adsorption capacity for Hg(II) of 580.0 mg/g was achieved using an initial concentration of 1500 mg/L and the maximum adsorption capacity for phosphate ions of 178.0 mg/g was achieved using an initial concentration of 1000 mg/L.

The theoretical Langmuir adsorption isotherm module was used to interpret the experimental data. The mathematical relationship of this module is shown in the following eq 5,[27,44] where q_e is the amount of the adsorbed gas per unit mass at equilibrium in (mg/g), C_e is the equilibrium concentration of the adsorbate in (mg/L), b is the Langmuir constant in (L/mg), and q_m is the Langmuir monolayer adsorption capacity in (mg/g).

$$\frac{C_e}{q_e} = \frac{1}{q_m}C_e + \frac{1}{bq_m} \tag{5}$$

$$R_L = \frac{1}{1 + bC_0} \tag{6}$$

The constant b can be used to calculate the R_L value, as shown in eq 6. This relation can be used to predict the shape of the isotherm to be either linear (R_L = 1), irreversible (R_L = 0), favorable (0 < R_L < 1), or unfavorable (R_L > 1).[27,44]

The results are plotted in Figure 6D for Hg(II) and $(HPO_4)^{2-}$ and they showed that the data fitted well with the Langmuir adsorption isotherm module due to the high values of (R^2). Moreover, the calculated theoretical data from the module and the experimental data showed excellent agreement with this module and the R_L values are between 0 and 1 indicate favorable adsorption, as summarized in Table 2.

Table 2. Langmuir Parameters for the Adsorption of Hg(II) and $(HPO_4)^{2-}$ Ions on UIO-66-IT

metal ion	R^2	b (L/mg)	$Q_{max,fitted}$	Q_{exp}	R_L
Hg(II)	0.994	0.026	587.5	580.0	0.0041
$(HPO_4)^{2-}$	0.999	0.049	181.8	178.0	0.0122

3.3.3. Effect of Contact Time and Adsorption Kinetics. The effect of contact time on the removal of Hg(II) and $(HPO_4)^{2-}$ on UIO-66-IT was studied using initial concentrations of 100 mg/L. The results are plotted in Figure 7A and they reveal that the contact times needed to achieve the maximum adsorption capacities were 30 and 45 min for Hg(II) and $(HPO_4)^{2-}$, respectively. The kinetics of the adsorption process indicates that more than 70% of the adsorption capacities of corresponding adsorbents occurred within 15 min for Hg(II) and 30 min for $(HPO_4)^{2-}$. This rapid initial increase in adsorption is likely due to the abundance of void adsorption sites on the surface of the UIO-66-IT adsorbent.

The pseudo-second-order module was used to explain heavy metal adsorption kinetics. Equation 7 represents the linear form of the pseudo-second-order kinetic module, which is used to calculate the rate constant of adsorption by plotting t/q_t on the y-axis as a function of time on the x-axis. The slope of the line is $(1/q_e)$, and the y-intercept is $(1/K_2q_e^2)$, and from the data, it is possible to calculate the rate constant and q_e and compare it with experimental data.

$$\frac{t}{q_t} = \frac{1}{q_e}t + \frac{1}{K_2q_e^2} \tag{7}$$

https://doi.org/10.1021/acs.iecr.1c01892
Ind. Eng. Chem. Res. 2021, 60, 12675−12688

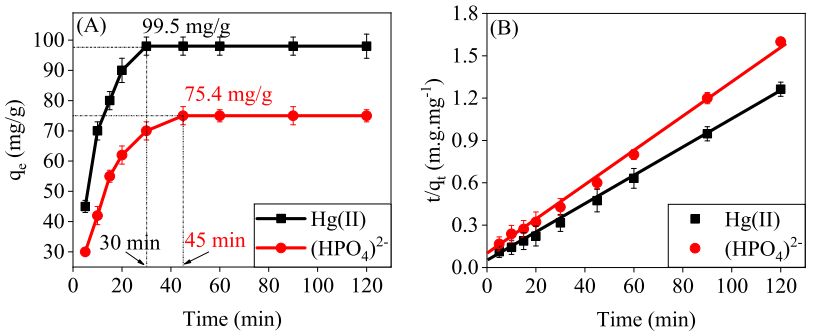

Figure 7. (A) Effect of contact time on the removal of Hg(II) and $(HPO_4)^{2-}$ on UIO-66-IT (conditions; C_0 = 100 mg/L, pH = 5.5, T = 298 K, dose = 5 mg/5 mL) and (B) pseudo-second-order kinetic module.

where k_2 (g/mol min) is the pseudo-second-order rate constant of adsorption and q_e, and q_t are the adsorbed amount (mg/g) at equilibrium and at time t (min), respectively.[27,44,45]

The pseudo-second-order kinetic model was used to analyze the experimental kinetic data, as shown in Figure 7B. The model fits quite well with the experimental data (correlation coefficient R^2 > 0.999). As shown in Table 3, the calculated maximum adsorption capacities of Hg(II) and $(HPO_4)^{2-}$ were in good agreement with the experimental results. Therefore, the adsorption occurs through the sharing or exchange of electrons between UIO-66-IT and Hg(II) and $(HPO_4)^{2-}$, resulting in the removal of the ions from water.

Table 3. Kinetic Parameters for the Adsorption of Hg(II) and $(HPO_4)^{2-}$ on the UIO-66-IT Adsorbent

metal ion	$q_{e,exp}$ (mg g^{-1})	$q_{e,calc}$ (mg g^{-1})	k_2 (g mol^{-1} min^{-1})	R^2
Hg(II)	99.50	98.52	0.003241	0.998
$(HPO_4)^{2-}$	75.40	80.46	0.001931	0.997

3.3.4. Effect of Temperature and Adsorption Thermodynamics. The effect of temperature on the adsorption capacities of Hg(II) and $(HPO_4)^{2-}$ ions using UIO-66-IT was studied using the following constant conditions (pH = 5.5, t = 6 h, dose = 5 mg/L, Hg(II) concentrations 5−1800 and 5−1000 mg/L for phosphate). The temperatures used for this study were 25, 35, and 50 °C. The results are depicted in Figure 8A,B for Hg(II) and $(HPO_4)^{2-}$, respectively. The results indicated that the maximum adsorption capacities of Hg(II) and $(HPO_4)^{2-}$ using UIO-66-IT increased from 580 to 740 and 178.0 to 256.2 mg/g, respectively, when the temperature increased from 25 to 55 °C. The mobility and kinetic energy of ions in solution increase at high temperatures and are likely responsible for the increase in the observed maximum adsorption capacities.[46]

The thermodynamic functions ($\Delta G°$, $\Delta H°$, and $\Delta S°$) of the adsorption were calculated using eqs 8 and 9, where $\Delta G°$ is the free energy change, $\Delta H°$ is the enthalpy change, $\Delta S°$ is the

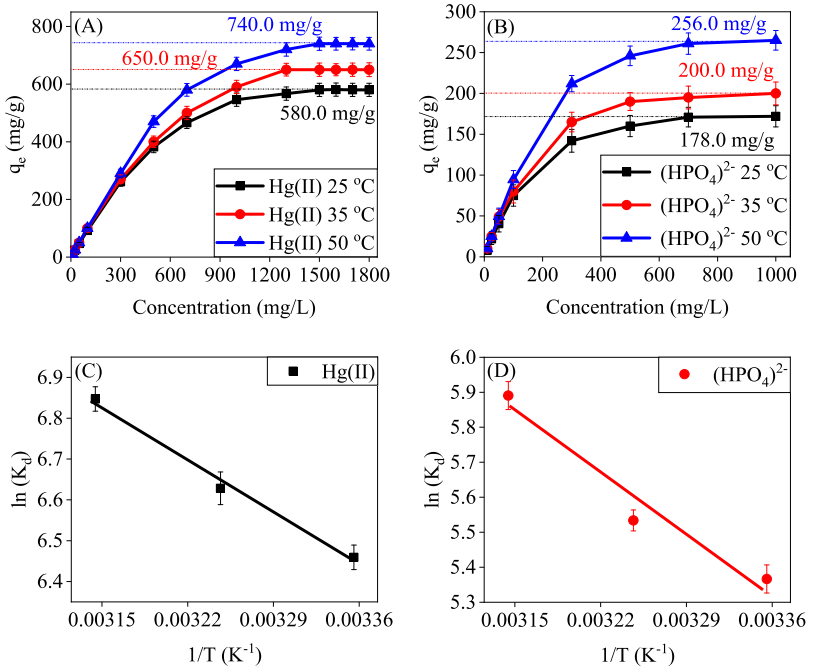

Figure 8. Effect of temperature on the removal of (A) Hg(II) and (B) $(HPO_4)^{2-}$ using UIO-66-IT [conditions; C_0 = 5−1800 mg/L Hg(II), 5−1000 mg/L $(HPO_4)^{2-}$, pH = 5.5, T = 25, 35, and 50 °C, t = 6 h, dose = 5 mg/5 mL]. (C,D) Plots of ln (K_d) vs T^{-1} for the estimation of the thermodynamics parameters of the adsorption process for Hg and $(HPO_4)^{2-}$, respectively.

https://doi.org/10.1021/acs.iecr.1c01892
Ind. Eng. Chem. Res. 2021, 60, 12675−12688

entropy change, R is the gas constant, T is the temperature, and K_c is the equilibrium constant.[27,46]

$$\Delta G^\circ = -RT \ln K_c \quad (8)$$

$$\ln K_c = \left(\frac{\Delta S^\circ}{R}\right) - \left(\frac{\Delta H^\circ}{R}\right)\frac{1}{T} \quad (9)$$

The data were plotted in Figure 8C,D for Hg(II) and $(HPO_4)^{2-}$, respectively, and the thermodynamics parameters are summarized in Table 4. The ΔG° values for both adsorbates are negative, indicating the spontaneous nature of the adsorption process. The positive value of ΔH° confirms the endothermic nature of the adsorption process, which is consistent with the increase in maximum adsorption capacity that occurs with the increasing temperature. The positive ΔS° values indicate an increase of disorder at the solid/solute interface during the adsorption process resulting from the liberation of water solvent molecules from the metal ion to the solution.[46]

Table 4. Thermodynamic Parameters for the Adsorption of Hg(II) and $(HPO_4)^{2-}$ on UIO-66-IT

metal ion	ΔG (kJ/mol)	ΔH (kJ/mol)	ΔS (kJ/mol·K)
Hg(II)	−40.2	25.4	0.21
$(HPO_4)^{2-}$	−30.5	87.6	0.29

3.3.5. Effect of Competitive Ions and Selectivity. Selective adsorption of Hg(II) by UIO-66-IT was studied using an ionic solution containing a variety of metal ions (Hg(II), Cu(II), Al(II), Fe(III), Zn(II), and Ni(II)) at 25 and 300 ppm. As depicted in Figure 9A, the adsorbent has high selectivity toward Hg among the mixture of metal ions at both concentrations. This can be explained using the hard soft acid base theory.[47] Because UIO-66-IT has S and N soft base elements, the adsorbent has a high affinity for soft acids but does not have an affinity for hard acids.[47]

Furthermore, the selectivity of UIO-66-IT on the removal of phosphate was studied in the presence of various anions and two sets of initial concentrations, as shown in Figure 9B. The results indicate that UIO-66-IT is not selective toward phosphate removal, but the removal efficiency is still high (100% at 500 ppb) even with the existence of interfering anions. Therefore, UIO-66-IT is considered to be an efficient adsorbent for the highly efficient and selective removal of Hg and the highly efficient removal of phosphate ions.

3.3.6. Effect of Adsorbent Dosage. The effect of adsorbent dosage on the removal of Hg(II) and $(HPO_4)^{2-}$ ions on UIO-66-IT was investigated at constant pH = 5, contact time = 6 h, temperature = 298 K, and concentration = 1000 mg/L for Hg(II) ions and 500 mg/L for $(HPO_4)^{2-}$ ions, while the amounts of the adsorbent were varied between 0.05 and 0.045 g. The results are plotted in Figure 10, and they showed that

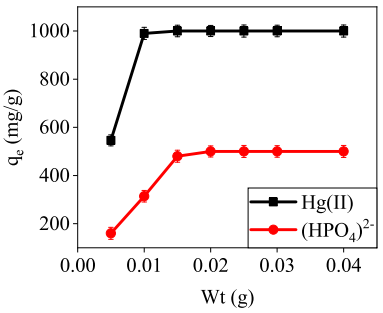

Figure 10. Effect of adsorbent dose on the removal of Hg(II) and $(HPO_4)^{2-}$ ions on UIO-66-IT [conditions: C_0 = 1000 mg/L Hg(II) and 500 mg/L $(HPO_4)^{2-}$; T = 298 K; pH = 5.5; adsorbent dose = 0.005−0.040 g/5 mL].

the uptake of Hg(II) and $(HPO_4)^{2-}$ ions increases significantly by increasing the dose of the adsorbent from 546 to 1000 mg/g for Hg(II) and from 160 to 500 mg/g for $(HPO_4)^{2-}$, by increasing the dose of UIO-66-IT from 0.005 to 0.040 g/L. This is attributed to the availability of more active sites at a higher dosage of UIO-66-IT, which can be used to extract a high amount of Hg(II) or $(HPO_4)^{2-}$ ions from the solutions.[48]

3.3.7. Proposed Mechanisms. The adsorption of mercury on the surface of UIO-66-IT takes place through the chelation mechanism, as depicted in Scheme 3A. However, the adsorption of phosphate ions on UIO-66-IT takes place through electrostatic interaction, as depicted in Scheme 3B. In the chelation mechanism, a covalent coordination bond can be generated between Lewis acids (heavy metals, which have vacant d-orbitals) and Lewis bases (atoms with a lone pair of electrons). Therefore, because UIO-66-IT has different active sites such as S and N, it is possible to act as Lewis bases and form stable coordination complexes with mercury ions in the solution, which acts as Lewis acids. The possible structures to chelate mercury are depicted in Scheme 4. However, the removal of phosphate takes place by two types of electrostatic interactions. The first one is between phosphate ions and amine or sulfur functional groups on the IT chelating ligand.

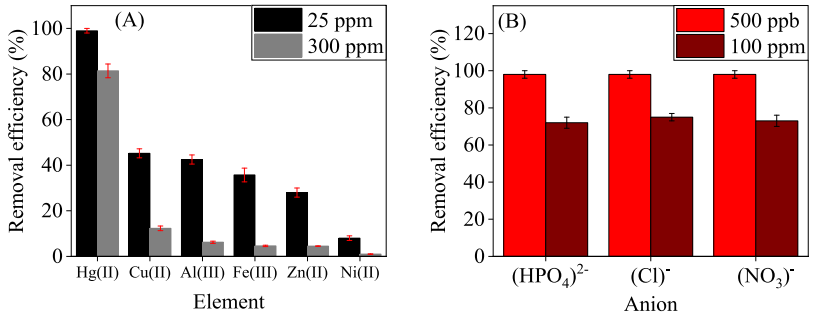

Figure 9. Effect of coexistence ions for the removal of (A) Hg(II) and (B) $(HPO_4)^{2-}$ on UIO-66-IT [conditions; C_0 = 25,300 ppm for Hg and interfering cations Cu(II), Al(III), Fe(III), Zn(II), and Ni(II), 500 and 100 ppm for $(HPO_4)^{2-}$ and interfering anions Cl^- and $(NO_3)^-$, T = 298, pH = 5, dose = 5 mg/5 mL].

https://doi.org/10.1021/acs.iecr.1c01892
Ind. Eng. Chem. Res. 2021, 60, 12675−12688

Scheme 3. Proposed Mechanisms for the Removal of (A) Hg(II) and (B) Phosphate Ions on UIO-66-IT

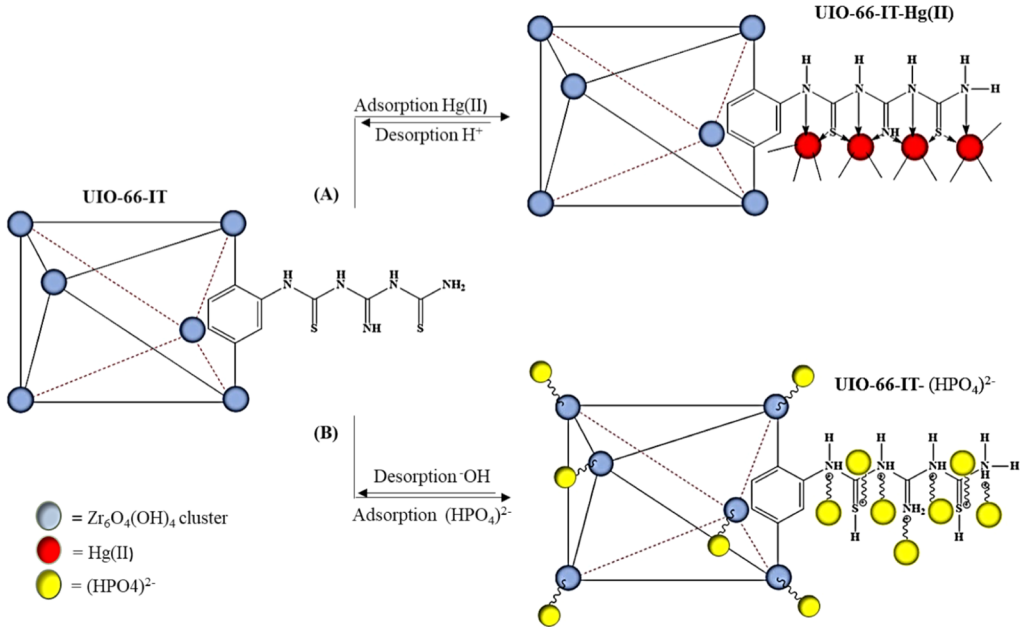

Scheme 4. Suggested Structures of Chelating Compounds of Hg(II) Ions on UIO-66-IT

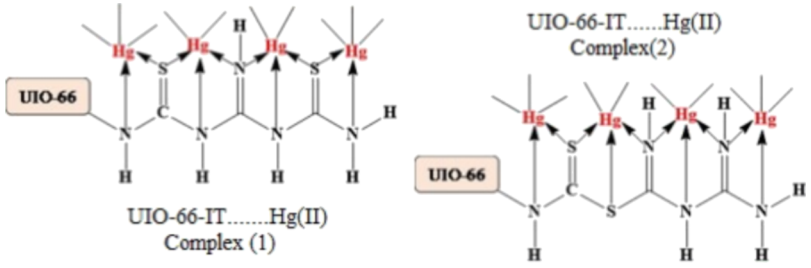

The second electrostatic interaction is between negatively charged phosphate ions and positively charged metal sites in the UIO-66-IT MOF as was reported somewhere else in the literature.[25,31,47]

XPS was used to prove the chelation of Hg(II) on UIO-66-IT. The survey spectrum of UIO-66-IT after Hg(II) removal is depicted in Figure 11A, and it showed, in addition to the UIO-66-IT peaks, a peak corresponding to the presence of mercury on UIO-66-IT. To get more information about mercury coordination from the solution, the high spectrum of Hg 4f was plotted, as shown in Figure 11B, and it showed two peaks at binding energy values of 100.9 and 104.8 eV for Hg $4f_{7/2}$ and Hg $4f_{5/2}$, respectively.[2,27] To confirm the chelation of Hg on UIO-66-IT, the spectra of N 1s and S 2p before and after Hg(II) chelation are plotted in Figure 11B,C. It can be clearly seen that after Hg adsorption, some peaks shifted to different binding energy values and some peaks have a significant change in their intensities, which can be used to explain the chelation mechanism. For example, N═C appeared at a binding energy value of 399.1 eV, but after Hg removal, the value shifted to 399.4 eV due to the formation of the (Hg−N═C) complex. Similarly, the C−S bond has a binding energy value of 162.2 eV, but after the removal of Hg(II), this peak moved to 161.6 eV due to the formation of the (Hg−S−C) bond.[2,26]

3.3.8. Desorption and Reusability Studies. The reusability of a new adsorbent is an important parameter that an efficient

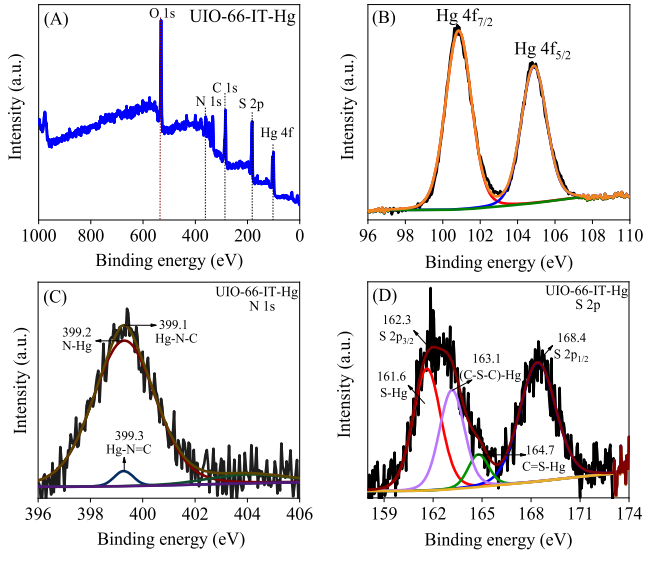

Figure 11. XPS spectra of UIO-66-IT after Hg removal (A) and survey spectrum of (B) Hg 4f, (C) N 1s, and (D) S 2p.

adsorbent should have. The results of desorption studies of both Hg(II) and $-(HPO_4)^{2-}$ ions from the surface of UIO-66-IT are summarized in Table 5. The 100% desorption of UIO-66-IT-Hg was accomplished by washing the adsorbent with 0.01 M hydrochloric acid, 1% thiourea, and DI water,

https://doi.org/10.1021/acs.iecr.1c01892
Ind. Eng. Chem. Res. 2021, 60, 12675−12688

Table 5. Desorption Studies of Hg(II), and $(HPO_4)^{2-}$ from UIO-66-IT Using Different Desorption Eluents

adsorbate	eluent	q_e (mg/g)	q_d (mg/g)	De (%)
50 mg/L Hg(II)	0.01 M HCl	50	20	40.00
	0.01 M HCl + 0.05% thiourea	50	35	70.00
	0.01 M HCl + 1% thiourea	50	50	100.00
50 mg/L $(HPO_4)^{2-}$	0.5% NaCl	50	28	56.00
	1% NaCl	50	50	100.00

respectively. However, the 100% desorption of UIO-66-IT-$(HPO_4)^{2-}$ was accomplished by washing the adsorbent with 1% sodium chloride and DI water. According to these results, it is possible to use UIO-66-IT several times to adsorb and desorb water contaminants because the desorption reaches 100% from the adsorbent surface. The recycling of the UIO-66-IT adsorbent for both Hg(II), and $(HPO_4)^{2-}$ is depicted in Figure 12. It is clearly seen that after six adsorption−

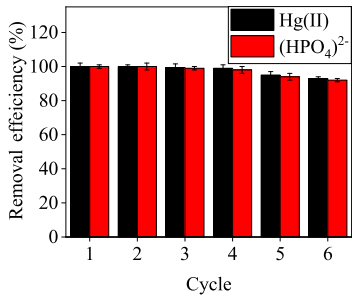

Figure 12. Recycling of the UIO-66-IT composite for Hg(II) (desorption condition: 0.01 M hydrochloric acid, 1% thiourea) and $(HPO_4)^{2-}$ (desorption condition: 1% HCl) dose: 1 g/L, initial concentration 50 mg/L.

desorption cycles, the adsorbent still has removal efficiency higher than 95%. These results prove that the UIO-66-IT adsorbent has tremendous reusability for both Hg(II), and $(HPO_4)^{2-}$ from aqueous solutions.

3.3.9. Comparing UIO-66-IT for Hg(II) Removal with Other Adsorbents. To prove the tremendous ability of UIO-66-IT to remove Hg(II) from aqueous solutions, Table 6 compares the maximum adsorption capacities for different UIO-66-MOFs and other reported adsorbents in the literature. The maximum adsorption capacity for UIO-66-IT was 580 mg/g achieved at pH 5.5 and 30 min contact time. This value was higher than all unfunctionalized and functionalized UIO-66 MOFs shown in Table 6 except for UIO-66-DMTD, which is 670 mg/g higher than our adsorbent. However, the UIO-66-DMTD adsorbent achieves this adsorbent capacity at a contact time of 180 min, which is longer than our adsorbent UIO-66-IT. Moreover, by looking at all UIO-66 MOFs shown in Table 6, it is clearly seen that as UIO-66 has chelating ligands that have different heteroatoms especially S and N, the adsorption capacity increased significantly. Also, by comparing our adsorbent to adsorbents, besides UIO-66 MOFs such as other MOFs, activated carbons, and GO as given in Table 6, our adsorbent has a higher adsorption capacity than all these adsorbents. These results confirm the tremendous ability of UIO-66-IT to remove Hg(II) ions from contaminated water.

Table 6. Comparison of the Adsorption Capacities of Hg(II) Ions onto Various Adsorbents

adsorbent	conditions			Q_e (mg/g)	refs
	pH	t (min)	T (K)		
UIO-66	4		298	59.30	27
UIO-66-NH_2	4		298	145.1	27
UIO-66-SO_3H	4		298	181.2	27
UIO-66-NCS	5	30	298	250.00	this work
UIO-66-$(SH)_2$	5	90	298	236.40	26
UIO-66-L-cysteine	5.0	180	303	350.14	28
UIO-66-IT	5.5	30	293	580.00	this work
UIO-66-DMTD	5.5	180	298	670.00	27
N-MPC-700-7/3	6.0	10	298	489.00	49
SH-MiL-68(In)	4.0	20	298	450.00	50
MNPC-T700-M3	4.0	20	298	429.00	51
Fe_3O_4-polypyrrole-GO	5.5	90	298	400.00	52
thiol-Zr-MOF	6.0	10	298	171.50	25
cyst-PRGO	5.3	60	293	169.00	53

3.3.10. Comparing UIO-66-IT for Phosphate Removal with Other Adsorbents. To prove the excellent removal ability of UIO-66-IT toward $(HPO_4)^{2-}$, comparison to the most reported adsorbent in the literature is made, as given in Table 7. The adsorption capacity of UIO-66-IT toward $(HPO_4)^{2-}$ is

Table 7. Comparison of the Adsorption Capacities of $(HPO_4)^{2-}$ Ions onto Various Adsorbents

adsorbent	conditions			Q_e (mg/g)	refs
	pH	t (min)	T (K)		
UIO-66-IT	5.5	45	298	187.00	this work
$Ce_{0.8}Zr_{0.2}O_2$	6.0	60	298	112.23	54
Mg−Al-LDH		250	298	102.67	55
PAN−NH_2−$La_{0.3}$	5.5	480	298	96.09	56
GO-Fe_2O_3	6.0	5	298	93.28	57
UIO-66-NH_2		20	293	92.00	31
UIO-66		20	293	85.00	31
GO-La-composite	6.2	25	293	82.60	58
Mg−Al-LDH		100	298	65.95	55
lignin-NH_2@Ce	5.0	60	298	27.86	59
Fe-HNT	4.0	480	298	5.46	60

187 mg/g, which is the highest value in the table compared to all listed adsorbents given in Table 7. This could be attributed to the presence of the IT chelating ligand, which has different S and N functional groups in addition to Zr that can act as active sites to capture phosphate ions from the solution. In addition to UIO-66-IT, the highest adsorption capacity can be accomplished at normal water pH and fast adsorption kinetics compared to the most reported adsorbents given in Table 7. This can reduce the cost and the time that are required to remove the phosphate ions from the solution. Therefore, UIO-66-IT is considered the best and efficient adsorbent to purify water from phosphate contaminants.

4. CONCLUSIONS

This work investigates the post-functionalization of UiO-66-NH_2 by a IT chelating ligand that was used to create a novel adsorbent for the removal of Hg(II) and phosphate ions from contaminated water. While the adsorbent removed Hg(II) and phosphate ions with high efficiencies, the Hg(II) ions were also removed with high selectivity. The maximum adsorption

https://doi.org/10.1021/acs.iecr.1c01892
Ind. Eng. Chem. Res. 2021, 60, 12675−12688

capacities of the UIO-66-IT adsorbent to Hg(II) and phosphate were 580.0 and 187.0 mg/g, respectively, at 25 °C and pH = 5.5, which was higher than UiO-66-SCN, UiO-66-NH_2, and other adsorbents reported in the literature. The experimental isotherm data were in good agreement with the Langmuir isotherm models, indicating that the monolayer adsorption of mercury and phosphate ions on the surface of the UIO-66-IT nanoadsorbent occurred on homogeneous surfaces and the adsorption mode belonged to chemisorption type. The adsorption kinetic results for both adsorbates matched with the pseudo-second-order kinetic model, and the removal rate was proportional to the square of the concentration of Hg(II) or $(H_3PO_4)^{2-}$. The mechanism of Hg(II) adsorption was the chelation mechanism between N and S active sites on the UIO-66-IT or electrostatic interaction mechanism between protonated functional groups and phosphate ions. UIO-66-IT has excellent reusability results, which make it a unique adsorbent to remediate polluted water from mercury and phosphate ions.

■ ASSOCIATED CONTENT

Supporting Information

The Supporting Information is available free of charge at https://pubs.acs.org/doi/10.1021/acs.iecr.1c01892.

XPS of UIO-66-NH_2, XPS spectra of UIO-66-NCS, SEM and TEM images of UIO-66-NH_2, and SEM and TEM images of UIO-66-NCS (PDF)

■ AUTHOR INFORMATION

Corresponding Authors

Ayyob M. Bakry − *Department of Chemistry, Virginia Commonwealth University, Richmond, Virginia 23284, United States; Department of Chemistry, Faculty of Science, Jazan University, Jizan 45142, Saudi Arabia;* orcid.org/0000-0003-4108-5963; Phone: 0173295000; Email: ayyob1986@gmail.com

M. Samy El-Shall − *Department of Chemistry, Virginia Commonwealth University, Richmond, Virginia 23284, United States;* orcid.org/0000-0002-1013-4948; Phone: 804-828-2753; Email: mselshal@vcu.edu; Fax: 804-828-8599

Authors

Fathi S. Awad − *Department of Chemistry, Virginia Commonwealth University, Richmond, Virginia 23284, United States; Chemistry Department, Faculty of Science, Mansoura University, Mansoura 35516, Egypt;* orcid.org/0000-0002-9907-0695

Amr Awad Ibrahim − *Department of Chemistry, Virginia Commonwealth University, Richmond, Virginia 23284, United States; Chemistry Department, Faculty of Science, Mansoura University, Mansoura 35516, Egypt;* orcid.org/0000-0002-1315-6616

Andrew Lin − *Department of Chemistry, Virginia Commonwealth University, Richmond, Virginia 23284, United States*

Complete contact information is available at: https://pubs.acs.org/10.1021/acs.iecr.1c01892

Notes

The authors declare no competing financial interest.

■ ACKNOWLEDGMENTS

We thank the National Science Foundation (CHE-1900094) for the support of this work.

■ REFERENCES

(1) Yadav, M.; Gupta, R.; Arora, G.; Yadav, P.; Srivastava, A.; Sharma, R. K. Current Status of Heavy Metal Contaminants and Their Removal/Recovery Techniques. *Contaminants in Our Water: Identification and Remediation Methods*; American Chemical Society, 2020; Vol. *1352*, pp 41−64.

(2) Awad, F. S.; AbouZeid, K. M.; El-Maaty, W. M. A.; El-Wakil, A. M.; El-Shall, M. S. Efficient Removal of Heavy Metals from Polluted Water with High Selectivity for Mercury(II) by 2-Imino-4-thiobiuret−Partially Reduced Graphene Oxide (IT-PRGO). *ACS Appl. Mater. Interfaces* **2017**, *9*, 34230−34242.

(3) Wu, B.; Wan, J.; Zhang, Y.; Pan, B.; Lo, I. M. C. Selective Phosphate Removal from Water and Wastewater using Sorption: Process Fundamentals and Removal Mechanisms. *Environ. Sci. Technol.* **2020**, *54*, 50−66.

(4) Chakraborty, R.; Asthana, A.; Singh, A. K.; Jain, B.; Susan, A. B. H. Adsorption of heavy metal ions by various low-cost adsorbents: a review. *Int. J. Environ. Anal. Chem.* **2020**, 1−38.

(5) Kommu, A.; Singh, J. K. A review on graphene-based materials for removal of toxic pollutants from wastewater. *Soft Mater.* **2020**, *18*, 297−322.

(6) Shi, Q.; Sterbinsky, G. E.; Prigiobbe, V.; Meng, X. Mechanistic Study of Lead Adsorption on Activated Carbon. *Langmuir* **2018**, *34*, 13565−13573.

(7) Musielak, M.; Gagor, A.; Zawisza, B.; Talik, E.; Sitko, R. Graphene Oxide/Carbon Nanotube Membranes for Highly Efficient Removal of Metal Ions from Water. *ACS Appl. Mater. Interfaces* **2019**, *11*, 28582−28590.

(8) Kundu, S.; Chowdhury, I. H.; Naskar, M. K. Nitrogen-Doped Nanoporous Carbon Nanospheroids for Selective Dye Adsorption and Pb(II) Ion Removal from Waste Water. *ACS Omega* **2018**, *3*, 9888−9898.

(9) Tang, Y.; Li, Y.; Zhang, Y.; Mu, C.; Zhou, J.; Zhang, W.; Shi, B. Nonswelling Silica−Poly(acrylic acid) Composite for Efficient and Simultaneous Removal of Cationic Dye, Heavy Metal, and Surfactant-Stabilized Emulsion from Wastewater. *Ind. Eng. Chem. Res.* **2020**, *59*, 3383−3393.

(10) Ge, Y.; Li, Z. Application of Lignin and Its Derivatives in Adsorption of Heavy Metal Ions in Water: A Review. *ACS Sustain. Chem. Eng.* **2018**, *6*, 7181−7192.

(11) Daochalermwong, A.; Chanka, N.; Songsrirote, K.; Dittanet, P.; Niamnuy, C.; Seubsai, A. Removal of Heavy Metal Ions Using Modified Celluloses Prepared from Pineapple Leaf Fiber. *ACS Omega* **2020**, *5*, 5285−5296.

(12) Zhao, G.; Huang, X.; Tang, Z.; Huang, Q.; Niu, F.; Wang, X. Polymer-based nanocomposites for heavy metal ions removal from aqueous solution: a review. *Polym. Chem.* **2018**, *9*, 3562−3582.

(13) Afshari, M.; Dinari, M.; Zargoosh, K.; Moradi, H. Novel Triazine-Based Covalent Organic Framework as a Superadsorbent for the Removal of Mercury(II) from Aqueous Solutions. *Ind. Eng. Chem. Res.* **2020**, *59*, 9116−9126.

(14) Huang, L.; Mao, N.; Yan, Q.; Zhang, D.; Shuai, Q. Magnetic Covalent Organic Frameworks for the Removal of Diclofenac Sodium from Water. *ACS Appl. Nano Mater.* **2020**, *3*, 319−326.

(15) Boix, G.; Troyano, J.; Garzón-Tovar, L.; Camur, C.; Bermejo, N.; Yazdi, A.; Piella, J.; Bastus, N. G.; Puntes, V. F.; Imaz, I.; Maspoch, D. MOF-Beads Containing Inorganic Nanoparticles for the Simultaneous Removal of Multiple Heavy Metals from Water. *ACS Appl. Mater. Interfaces* **2020**, *12*, 10554−10562.

(16) Ma, X.; Chai, Y.; Li, P.; Wang, B. Metal−Organic Framework Films and Their Potential Applications in Environmental Pollution Control. *Acc. Chem. Res.* **2019**, *52*, 1461−1470.

(17) Kobielska, P. A.; Howarth, A. J.; Farha, O. K.; Nayak, S. Metal−organic frameworks for heavy metal removal from water. *Coord. Chem. Rev.* **2018**, *358*, 92−107.
(18) Sun, D. T.; Peng, L.; Reeder, W. S.; Moosavi, S. M.; Tiana, D.; Britt, D. K.; Oveisi, E.; Queen, W. L. Rapid, Selective Heavy Metal Removal from Water by a Metal−Organic Framework/Polydopamine Composite. *ACS Cent. Sci.* **2018**, *4*, 349−356.
(19) Schoenecker, P. M.; Carson, C. G.; Jasuja, H.; Flemming, C. J. J.; Walton, K. S. Effect of water adsorption on retention of structure and surface area of metal−organic frameworks. *Ind. Eng. Chem. Res.* **2012**, *51*, 6513−6519.
(20) Ahmadijokani, F.; Mohammadkhani, R.; Ahmadipouya, S.; Shokrgozar, A.; Rezakazemi, M.; Molavi, H.; Aminabhavi, T. M.; Arjmand, M. Superior chemical stability of UiO-66 metal-organic frameworks (MOFs) for selective dye adsorption. *Chem. Eng. J.* **2020**, *399*, 125346.
(21) Molavi, H.; Hakimian, A.; Shojaei, A.; Raeiszadeh, M. Selective dye adsorption by highly water stable metal-organic framework: Long term stability analysis in aqueous media. *Appl. Surf. Sci.* **2018**, *445*, 424−436.
(22) Ahmadijokani, F.; Tajahmadi, S.; Bahi, A.; Molavi, H.; Rezakazemi, M.; Ko, F.; Aminabhavi, T. M.; Arjmand, M. Ethylenediamine-functionalized Zr-based MOF for efficient removal of heavy metal ions from water. *Chemosphere* **2021**, *264*, 128466.
(23) Zhao, P.; Liu, N.; Jin, C.; Chen, H.; Zhang, Z.; Zhao, L.; Cheng, P.; Chen, Y. UiO-66: An Advanced Platform for Investigating the Influence of Functionalization in the Adsorption Removal of Pharmaceutical Waste. *Inorg. Chem.* **2019**, *58*, 8787−8792.
(24) Winarta, J.; Shan, B.; McIntyre, S. M.; Ye, L.; Wang, C.; Liu, J.; Mu, B. A Decade of UiO-66 Research: A Historic Review of Dynamic Structure, Synthesis Mechanisms, and Characterization Techniques of an Archetypal Metal−Organic Framework. *Cryst. Growth Des.* **2020**, *20*, 1347−1362.
(25) Ding, L.; Luo, X.; Shao, P.; Yang, J.; Sun, D. Thiol-Functionalized Zr-Based Metal−Organic Framework for Capture of Hg(II) through a Proton Exchange Reaction. *ACS Sustainable Chem. Eng.* **2018**, *6*, 8494−8502.
(26) Leus, K.; Perez, J. P. H.; Folens, K.; Meledina, M.; Van Tendeloo, G.; Du Laing, G.; Van Der Voort, P. UiO-66-(SH)2 as stable, selective and regenerable adsorbent for the removal of mercury from water under environmentally-relevant conditions. *Faraday Discuss.* **2017**, *201*, 145−161.
(27) Fu, L.; Wang, S.; Lin, G.; Zhang, L.; Liu, Q.; Fang, J.; Wei, C.; Liu, G. Post-functionalization of UiO-66-NH2 by 2,5-Dimercapto-1,3,4-thiadiazole for the high efficient removal of Hg(II) in water. *J. Hazard. Mater.* **2019**, *368*, 42−51.
(28) Zhao, M.; Huang, Z.; Wang, S.; Zhang, L.; Zhou, Y. Design of l-Cysteine Functionalized UiO-66 MOFs for Selective Adsorption of Hg(II) in Aqueous Medium. *ACS Appl. Mater. Interfaces* **2019**, *11*, 46973−46983.
(29) Saleem, H.; Rafique, U.; Davies, R. P. Investigations on post-synthetically modified UiO-66-NH2 for the adsorptive removal of heavy metal ions from aqueous solution. *Microporous Mesoporous Mater.* **2016**, *221*, 238−244.
(30) Liu, F.; Xiong, W.; Feng, X.; Cheng, G.; Shi, L.; Chen, D.; Zhang, Y. Highly recyclable cysteamine-modified acid-resistant MOFs for enhancing Hg (II) removal from water. *Environ. Technol.* **2020**, *41*, 3094−3104.
(31) Lin, K.-Y. A.; Chen, S.-Y.; Jochems, A. P. Zirconium-based metal organic frameworks: Highly selective adsorbents for removal of phosphate from water and urine. *Mater. Chem. Phys.* **2015**, *160*, 168−176.
(32) Qiu, H.; Yang, L.; Liu, F.; Zhao, Y.; Liu, L.; Zhu, J.; Song, M. Highly selective capture of phosphate ions from water by a water stable metal-organic framework modified with polyethyleneimine. *Environ. Sci. Pollut. Res. Int.* **2017**, *24*, 23694−23703.
(33) Guan, T.; Li, X.; Fang, W.; Wu, D. Efficient removal of phosphate from acidified urine using UiO-66 metal-organic frameworks with varying functional groups. *Appl. Surf. Sci.* **2020**, *501*, 144074.
(34) Tian, H.; Guo, J.; Pang, Z.; Hu, M.; He, J. A sulfur, nitrogen dual-doped porous graphene nanohybrid for ultraselective Hg(ii) separation over Pb(ii) and Cu(ii). *Nanoscale* **2020**, *12*, 16543.
(35) Štrukil, V. Mechanochemical synthesis of thioureas, ureas and guanidines. *Beilstein J. Org. Chem.* **2017**, *13*, 1828−1849.
(36) Hermanson, G. T. The Reactions of Bioconjugation. In *Bioconjugate Techniques*, 3rd ed.; Hermanson, G. T., Ed.; Academic Press: Boston, 2013; Chapter 3, pp 229−258.
(37) Ali-Moussa, H.; Navarro Amador, R.; Martinez, J.; Lamaty, F.; Carboni, M.; Bantreil, X. Synthesis and post-synthetic modification of UiO-67 type metal-organic frameworks by mechanochemistry. *Mater. Lett.* **2017**, *197*, 171−174.
(38) Shayegan, H.; Ali, G. A. M.; Safarifard, V. Recent Progress in the Removal of Heavy Metal Ions from Water Using Metal-Organic Frameworks. *ChemistrySelect* **2020**, *5*, 124−146.
(39) McGuire, C. V.; Forgan, R. S. The surface chemistry of metal−organic frameworks. *Chem. Commun.* **2015**, *51*, 5199−5217.
(40) Burke, B. P.; Seemann, J.; Archibald, S. J. Advanced Chelator Design for Metal Complexes in Imaging Applications: Radiopharmaceuticals, Protein Targeting, and Conjugation. In *Advances in Inorganic Chemistry*; van Eldik, R., Hubbard, C. D., Eds.; Academic Press, 2016; Vol. *68*, Chapter 7, pp 301−339.
(41) Golpour, M.; Pakizeh, M. Preparation and characterization of new PA-MOF/PPSU-GO membrane for the separation of KHI from water. *Chem. Eng. J.* **2018**, *345*, 221−232.
(42) Vellingiri, K.; Deep, A.; Kim, K.-H.; Boukhvalov, D.; Kumar, P.; Yaoa, Q. The sensitive detection of formaldehyde in aqueous media using zirconium-based metal organic frameworks. *Sensor. Actuator. B Chem.* **2017**, *241*, 938.
(43) Zhu, J.; Wu, L.; Bu, Z.; Jie, S.; Li, B.-G. Polyethyleneimine-Modified UiO-66-NH_2 (Zr) Metal−Organic Frameworks: Preparation and Enhanced CO_2 Selective Adsorption. *ACS Omega* **2019**, *4*, 3188−3197.
(44) Geisse, A. R.; Ngule, C. M.; Genna, D. T. Removal of Lead Ions from Water Using Thiophene-functionalized Metal-organic Frameworks. *Chem. Commun.* **2019**, *56*, 237.
(45) Sun, Q.; Aguila, B.; Perman, J.; Earl, L. D.; Abney, C. W.; Cheng, Y.; Wei, H.; Nguyen, N.; Wojtas, L.; Ma, S. Postsynthetically Modified Covalent Organic Frameworks for Efficient and Effective Mercury Removal. *J. Am. Chem. Soc.* **2017**, *139*, 2786−2793.
(46) Awad, F. S.; Abouzeid, K. M.; Abou El-Maaty, W. M.; El-Wakil, A. M.; El-Shall, M. S. Effective Removal of Mercury(II) from Aqueous Solutions by Chemically Modified Graphene Oxide Nanosheets. *Arabian J. Chem.* **2020**, *13*, 2659.
(47) Hu, H.; He, H.; Zhang, J.; Hou, X.; Wu, P. Optical sensing at the nanobiointerface of metal ion−optically-active nanocrystals. *Nanoscale* **2018**, *10*, 5035−5046.
(48) Ariffin, N.; Abdullah, M. M. A. B.; Mohd Arif Zainol, M. R. R.; Murshed, M. F.; Hariz, Z.; Faris, M. A.; Bayuaji, R. Review on Adsorption of Heavy Metal in Wastewater by Using Geopolymer. *MATEC Web Conf.* **2017**, *97*, 01023.
(49) Xu, D.; Lu, H.; Huang, Q.; Deng, B.; Li, L. Flame-retardant effect and mechanism of melamine phosphate on silicone thermoplastic elastomer. *RSC Adv.* **2018**, *8*, 5034−5041.
(50) Li, G.-P.; Zhang, K.; Zhang, P.-F.; Liu, W.-N.; Tong, W.-Q.; Hou, L.; Wang, Y.-Y. Thiol-Functionalized Pores via Post-Synthesis Modification in a Metal−Organic Framework with Selective Removal of Hg(II) in Water. *Inorg. Chem.* **2019**, *58*, 3409−3415.
(51) Huang, L.; He, M.; Chen, B.-b.; Cheng, Q.; Hu, B. Highly Efficient Magnetic Nitrogen-Doped Porous Carbon Prepared by One-Step Carbonization Strategy for Hg^{2+} Removal from Water. *ACS Appl. Mater. Interfaces* **2017**, *9*, 2550−2559.
(52) Zhou, C.; Zhu, H.; Wang, Q.; Wang, J.; Cheng, J.; Guo, Y.; Zhou, X.; Bai, R. Adsorption of mercury(ii) with an Fe_3O_4 magnetic polypyrrole−graphene oxide nanocomposite. *RSC Adv.* **2017**, *7*, 18466−18479.

(53) Yap, P. L.; Kabiri, S.; Tran, D. N. H.; Losic, D. Multifunctional Binding Chemistry on Modified Graphene Composite for Selective and Highly Efficient Adsorption of Mercury. *ACS Appl. Mater. Interfaces* **2019**, *11*, 6350−6362.
(54) Su, Y.; Yang, W.; Sun, W.; Li, Q.; Shang, J. K. Synthesis of mesoporous cerium−zirconium binary oxide nanoadsorbents by a solvothermal process and their effective adsorption of phosphate from water. *Chem. Eng. J.* **2015**, *268*, 270−279.
(55) Maia, M. A.; Dotto, G. L.; Perez-Lopez, O. W.; Gutterres, M. Phosphate removal from industrial wastewaters using layered double hydroxides. *Environ. Technol.* **2021**, *42*, 3095−3105.
(56) Koh, K. Y.; Zhang, S.; Chen, J. P. Improvement of Ultrafiltration for Treatment of Phosphorus-Containing Water by a Lanthanum-Modified Aminated Polyacrylonitrile Membrane. *ACS Omega* **2020**, *5*, 7170−7181.
(57) Bai, L.; Yuan, L.; Ji, Y.; Yan, H. Effective Removal of Phosphate from Aqueous by Graphene Oxide Decorated with $\alpha\alpha$-Fe_2O_3: Kinetic, Isotherm, Thermodynamic and Mechanism Study. *Arabian J. Sci. Eng.* **2018**, *43*, 3611.
(58) Chen, M.; Huo, C.; Li, Y.; Wang, J. Selective Adsorption and Efficient Removal of Phosphate from Aqueous Medium with Graphene−Lanthanum Composite. *ACS Sustain. Chem. Eng.* **2016**, *4*, 1296−1302.
(59) Liu, X.; He, X.; Zhang, J.; Yang, J.; Xiang, X.; Ma, Z.; Liu, L.; Zong, E. Cerium oxide nanoparticle functionalized lignin as a nano-biosorbent for efficient phosphate removal. *RSC Adv.* **2020**, *10*, 1249−1260.
(60) Almasri, D. A.; Saleh, N. B.; Atieh, M. A.; McKay, G.; Ahzi, S. Adsorption of phosphate on iron oxide doped halloysite nanotubes. *Sci. Rep.* **2019**, *9*, 3232.

https://doi.org/10.1021/acs.iecr.1c01892
Ind. Eng. Chem. Res. 2021, 60, 12675−12688